# Effects of two vibrational modes in the dissociative electron attachment to $CF_3Cl$

Michal Tarana,[1,2,*] Pawel Wielgus,[3] Szczepan Roszak,[3] and Ilya I. Fabrikant[2,†]
[1]*Institute of Theoretical Physics, Faculty of Mathematics and Physics, Charles University in Prague, V Holešovičkách 2, 18000 Prague, Czech Republic*
[2]*Department of Physics and Astronomy, University of Nebraska, 510 Stadium Drive, Lincoln, Nebraska 68588, USA*
[3]*Institute of Physical and Theoretical Chemistry, Wroclaw University of Technology, Wyb. Wyspianskiego 27, 50-370 Wroclaw, Poland*
(Received 23 March 2009; published 28 May 2009)

We present a study of multimode effects in dissociative electron attachment to $CF_3Cl$ molecules using a time-independent version of the local complex potential theory. Symmetric stretch C-Cl vibrations $\nu_3$ and symmetric deformation (or so-called umbrella) vibrations $\nu_2$ are included. The neutral and anion potential energy surfaces are calculated using the second-order Møller-Plesset perturbation theory with an empirical adjustment of the vertical attachment energy. The final-state vibrational distribution in the $CF_3(\nu_2)$ fragment is dominated by the $\nu_2=2$ state. We also find an increase in the total cross section as compared with the one-dimensional calculations. This is explained by an increase in the anion survival probability.

DOI: 10.1103/PhysRevA.79.052712 PACS number(s): 34.80.Ht, 34.80.Lx

## I. INTRODUCTION

Almost all of the dissociative electron attachment (DEA) calculations performed so far include only one vibrational mode representing the reaction coordinate. To the best of our knowledge, the only three exceptions are model calculations of the DEA to $CO_2$ [1], *ab initio* calculations for water [2], and recent study of the DEA to the $C_2H_2$ molecule [3]. All these calculations were carried out within the framework of the local complex potential (LCP) theory. In view of the tremendous amount of computational work necessary to obtain multidimensional complex potential energy surfaces and the solution of the multidimensional Schrödinger equation for the nuclear motion, it is apparent that the way to solve the DEA problems for molecules with more than three atoms is to make further (in addition to local) approximations. The one most common is to "freeze" all modes other than one corresponding to the reaction coordinate. Many calculations for polyatomic molecules have been performed in this way. However, the role of other modes in these calculations has not been investigated so far. The mode coupling effects are well known in molecular spectroscopy and photodissociation dynamics, but they are relatively less studied in DEA processes. In particular, it is not clear if all the other coordinates should be fixed in these calculations or optimized (in terms of the least energy value). According to the Franck-Condon principle, the nuclear geometry should not change during the electron capture, therefore from this point of view other coordinates should not be optimized, but rather fixed at the values corresponding to the nuclear configuration of the neutral molecule. However, after the initial capture, when two fragments (anion and neutral radical) separate, all nuclear coordinates evolve.

This paper presents an attempt to solve this problem for polyatomic molecules. We have chosen $CF_3Cl$ to study the resonance process

$$e + CF_3Cl(\nu_2, \nu_3) \rightarrow CF_3Cl^- \rightarrow CF_3(\nu_2') + Cl^-. \quad (1)$$

Here $\nu_2$ and $\nu_3$ stand for the symmetric deformation vibrations (so-called "umbrella" mode) and the symmetric stretch vibrations, $\nu_2'$, represent the umbrella mode of the free $CF_3$ radical. At this point we restrict our considerations to one mode only, in addition to the reaction mode $\nu_3$. This restriction can be justified by the same reasoning as that given by Shapiro and Bershon [4] in their studies of photodissociation of $CH_3I$. First, the intermediate anionic state responsible for the DEA at low energies has $A_1$ symmetry, therefore degenerate vibrations $\nu_4$, $\nu_5$, and $\nu_6$ of the $e$ type can be excited resonantly only in pairs. (They can also be excited directly due to the transition dipole moment, but this should not significantly affect the pure resonant DEA process.) Second, the C-F bond length $R_{FC}=1.34$ Å [5] is very close to that for the anion, 1.37 Å [5] and free $CF_3$ radical, 1.32 Å [6]. Therefore, we can assume that the C-F symmetric stretching mode $\nu_1$ is unlikely to be excited as well. These assumptions are confirmed by measurements of Mann and Linder [7] who observed strong electron-impact vibrational excitation of the $\nu_3$ and $\nu_2$ modes in the $A_1$ resonance region, whereas other modes were not significantly excited.

Inclusion of additional vibrational modes in description of the DEA to $CF_3Cl$ is of interest due to two reasons. First, it allows us to study the distribution of the internal energy of the fragment, in our case the energy of the umbrella mode in the $CF_3$ radical. This energy can be significant due to a large Franck-Condon factor of the transition from the initial vibrational state of $CF_3Cl$ to the excited umbrella vibrational mode of the intermediate anion $CF_3Cl^-$ or due to the final-state interaction between $Cl^-$ and $CF_3$ redistributing the internal energy of $CF_3$. Studies of the Rydberg electron attachment to $CH_3I$, $CF_3I$, and $CF_3Br$ molecules [8] showed that at high principal quantum number $n$ (or at low electron energies) the major portion of the energy released by electron capture appears in translation, indicating insignificance of the internal energy redistribution in the final state. However, at lower $n$ (or higher electron energies) the final-state interaction becomes important [9–11], although there are no

*tarana@mbox.troja.mff.cuni.cz
†iif@unlserve.unl.edu

 

quantitative theoretical or experimental results of the radical fragment internal energy redistribution.

The second motivation for study of the DEA with inclusion of the vibrational umbrella mode is the strong sensitivity of the DEA cross section to the initial vibrational state of the target or to the initial vibrational temperature. The one-mode approximation explains quite well the observed temperature dependence of the DEA in electron collisions with methyl halides [12,13]. However, it fails [14,15] to give the correct quantitative description of the observed temperature dependence [16] of the low-energy peak in the DEA to $CF_3Cl$. Recent joint experimental and theoretical work on the DEA to $CF_3Br$ [17] demonstrates that the DEA rate calculated in the one-mode approximation gives a slower growth at high temperatures than that observed. This indicates that the umbrella mode in perfluoromethyl halides is more important than in methyl halides. This is consistent with the fact that corresponding vibrational quanta are lower in perfluoromethyl halides (e.g., compare 168 meV in $CH_3Cl$ with 97 meV in $CF_3Cl$). Therefore, the excited umbrella mode is more populated there than in methyl halides.

The aim of this work is to study the effects of additional vibrational mode in the DEA to the $CF_3Cl$ molecule and to compare the results with the one-dimensional treatment. In all our calculations we are using a model resonance width from the previous one-dimensional calculations [14] which is arbitrarily, although reasonably, extended to two dimensions. Because of this model approach, we do not expect the present calculations to improve the quantitative agreement with experimental data. Rather, we aim to investigate the effect of the additional vibrational mode on the final-state energy distribution and the magnitude of the total cross section.

This paper is organized as follows: In Sec. II we describe our theoretical model and methods used to solve the corresponding equations, in Sec. III we describe the potentials used in our calculations, and in Sec. IV we discuss the results of the two-dimensional and one-dimensional calculations. Atomic units are used throughout the paper.

## II. THEORETICAL APPROACH

In the present work we employ the LCP theory [18–20] of the DEA. Since the nonlocal calculations are rather complicated even in the one-dimensional case, it is desirable to get the results using a simpler approach as a first step. In addition, the $A_1$ shape resonance in $CF_3Cl$ appears at a relatively high energy 1.83 eV [21] and it is rather narrow (the width about 0.6 eV). This justifies the use of the local theory for $CF_3Cl$. Another justification is given by the comparison of our local calculations with previously published nonlocal results [14,15] as discussed below in Sec. IV A.

### A. Coordinates and Hamiltonian

In our calculations the potential energy surfaces $V$ and $U$ for the neutral molecule $CF_3Cl$ and the anion $CF_3Cl^-$ are represented using two coordinates: C-Cl internuclear separation $R$ and the distance between the C atom and the plane formed by the fluorine atoms $r=-R_{CF}\cos\theta$, where $\theta$ is the F-C-Cl angle and $R_{FC}$ is the F-C bond length. Since we do not include the C-F stretching mode into our considerations, $R_{CF}$ is fixed and set to the value 1.342 Å corresponding to the equilibrium geometry of the neutral $CF_3Cl$. We take all the potentials relatively to the equilibrium potential energy of the neutral molecule. Asymptotically ($R\to\infty$) both surfaces are represented by the harmonic approximation $D_e+k(r-r_m)^2/2$ for the neutral molecule and $D_e+k(r-r_m)^2/2-E_A$ for the anion, where $k$ and $r_m$ are the force constant of the umbrella mode and equilibrium value of $r$ for the free $CF_3$ radical, $D_e$ is the dissociation energy of the C-Cl bond, and $E_A$ is the electron affinity of the Cl atom.

The classical kinetic energy for the nuclear motion taking into account the degrees of freedom described above can be derived from the general Hamiltonian for $XY_3Z$ molecules [22] by fixing of all variables except $R$ and $r$. In addition, we assume in the present work that the approximation of harmonic oscillations with small amplitude is suitable for the $CF_3$ umbrella motion. In principle, the angle $\theta_0$ corresponding to the equilibrium geometry of the $CF_3$ radical at given $R$ changes with the C-Cl distance. However, the potential surfaces show that this dependence is rather weak and enables us to assume that $\theta_0$ is constant and take its value at the equilibrium geometry of the neutral $CF_3Cl$. Then we can write the classical kinetic energy in the following form:

$$T=\frac{1}{2}\mu_\rho\dot{R}^2+\frac{3}{2}m_F\left(\cot^2\theta_0+\frac{m_C+m_{Cl}}{M}\right)\dot{r}^2+\frac{3m_{Cl}m_F}{M}\dot{R}\dot{r}, \tag{2}$$

where $m_C$, $m_{Cl}$, and $m_F$ are the masses of corresponding atoms, $M=m_C+m_{Cl}+3m_F$ is the total mass of the molecule, and $\mu_\rho=m_{Cl}(m_C+3m_F)/M$ is the reduced mass for the relative motion of the Cl atom and the $CF_3$ radical. All our calculations were performed in the following reaction coordinates [4] $\rho$ and $r$ which decouple kinetic energy (2),

$$\rho=R+\eta r,\quad \eta=\frac{3m_F}{m_C+3m_F}, \tag{3}$$

and $r$ remains unchanged. The reaction coordinate $\rho$ is simply the distance between the center of mass of the $CF_3$ radical and the Cl atom. Corresponding linear operator of the kinetic energy can be written in the reaction coordinates as follows:

$$T_\rho+T_r=-\frac{1}{2\mu_\rho}\frac{\partial^2}{\partial\rho^2}-\frac{1}{2\mu_r}\frac{\partial^2}{\partial r^2}, \tag{4}$$

where

$$\mu_r=3m_F\left(\cot^2\theta_0+\frac{m_C}{m_C+3m_F}\right). \tag{5}$$

As long as we are not dealing with the DEA to $CF_3Cl$ in vibrationally highly excited states, we can use the harmonic approximation for $V(\rho,r)$ and diagonalize the Hamiltonian $H=T_\rho+T_r+V$. This gives us the normal frequencies and

normal-mode coordinates expressed as linear combinations of $\rho-(R_0+\eta r_0)$ and $r-r_0$, where $R_0$ and $r_0$ are the equilibrium coordinates of the neutral molecule.

### B. Local theory of the dissociative electron attachment

We start the derivation of the formula for the DEA cross sections using the basic equation for the nuclear wave function $\chi_E(\rho,r)$ in the LCP approximation [18,19]:

$$[T_\rho + T_r + U(\rho,r) - i\Gamma(\rho,r)/2 - E]\chi_E(\rho,r) = V_{dk}(\rho,r)\zeta_i(\rho,r), \tag{6}$$

where $V_{dk}(\rho,r)=\sqrt{\Gamma(\rho,r)/2\pi}$ is the amplitude for electron capture into the resonance state, $\zeta_i(\rho,r)$ is the vibrational wave function of the neutral molecule in the initial state, and $U(\rho,r)$ represents the anionic potential surface.

To solve Eq. (6), we expand $\chi_E(\rho,r)$ in a basis depending on $r$ only [4]. Specifically, we select the eigenfunctions of the vibrational Hamiltonian for the $CF_3$ fragment [note that $\Gamma(\infty,r)=0$]:

$$[T_r + V^{\mathrm{h}}(\infty,r) - \epsilon_\nu]\phi_\nu(r) = 0, \tag{7}$$

where $\epsilon_\nu$ are the corresponding eigenenergies $\epsilon_\nu=D_e+\omega_2^f(\nu+1/2)$, $\omega_2^f$ is the harmonic frequency of the $CF_3$ radical umbrella mode, and $V^{\mathrm{h}}(\infty,r)$ is the corresponding free $CF_3$ radical potential curve in the harmonic approximation with the minimum corresponding to the C-Cl bond dissociation energy. Thus, the expansion has the form

$$\chi_E(\rho,r) = \sum_\nu \psi_\nu(\rho)\phi_\nu(r). \tag{8}$$

Projection of Eq. (6) on the functions $\phi_\nu(r)$ yields the following system of coupled differential equations for functions $\psi_\nu(\rho)$:

$$[T_\rho + \epsilon_\nu - E]\psi_\nu(\rho) + \sum_{\nu'} U_{\nu\nu'}(\rho)\psi_{\nu'}(\rho) = \lambda_{i\nu}(\rho), \tag{9}$$

where

$$U_{\nu\nu'}(\rho) = \int \phi_\nu(r)[U(\rho,r) - i\Gamma(\rho,r)/2 - V^{\mathrm{h}}(\infty,r)]\phi_{\nu'}(r)dr, \tag{10}$$

$$\lambda_{i\nu}(\rho) = \int V_{dk}(\rho,r)\zeta_i(\rho,r)\phi_s(r)dr. \tag{11}$$

Expansion (8) defines the channels corresponding to the vibrational states of the free $CF_3$ radical. We solve system of equations (9) with the outgoing-wave boundary condition at $\rho\to\infty$,

$$\frac{d\psi_\nu(\rho)}{d\rho} \sim iK_\nu\psi_\nu(\rho), \tag{12}$$

where $K_\nu^2=2\mu_\rho(E-\epsilon_\nu)$. In case of the energetically closed channels we take the asymptotically decaying condition. The DEA cross section corresponding to the $CF_3$ fragment in the vibrational state with the quantum number $\nu$ can be written as follows [18–20]:

$$\sigma_\nu = \frac{2\pi^2}{k^2}\frac{K_\nu}{\mu_\rho}\lim_{\rho\to\infty}|\psi_\nu(\rho)|^2, \tag{13}$$

where $k^2/2$ is the initial electron energy. As it is well known, Eq. (13) is not consistent with the Wigner threshold law at small electron energies. To repair this deficiency of the local theory, we introduce an additional correction factor [20,23] into the capture amplitude $V_{dk}(\rho,r)$:

$$c(\rho,r) = \begin{cases} \left(\dfrac{k^2}{2E_r(\rho,r)}\right)^\tau & k^2 < 2E_r(\rho,r) \\ 1 & \text{otherwise}, \end{cases} \tag{14}$$

where $\tau$ is the threshold exponent and $E_r(\rho,r)$ is the resonance energy discussed below. For $s$-wave capture in the absence of the dipole moment, $\tau=1/4$. It should be slightly modified for $CF_3Cl$. However, this correction becomes important only in the energy region close to the threshold. Our calculations showed that it does not play any significant role in the energy interval of our interest.

System of equations (9) can be solved efficiently using the Green's function for the homogeneous equations. Taking into account asymptotic condition (12), the column vector $\boldsymbol{\psi}(\rho)$ of the solutions $\psi_\nu(\rho)$ can be written in the following matrix form:

$$\boldsymbol{\psi}(\rho) = \frac{1}{2i\mu_\rho}\left\{\boldsymbol{\psi}^{(\mathrm{r})}(\rho)\int_\rho^\infty \boldsymbol{\psi}^{(+)T}(\rho')\boldsymbol{\lambda}(\rho')d\rho' + \boldsymbol{\psi}^{(+)}(\rho) \times \int_0^\rho \boldsymbol{\psi}^{(\mathrm{r})T}(\rho')\boldsymbol{\lambda}(\rho')d\rho'\right\}, \tag{15}$$

where $\boldsymbol{\lambda}(\rho)$ is the column vector of the source terms (11), the symbol $T$ means transposition of the corresponding matrix, and $\boldsymbol{\psi}^{(\mathrm{r})}(\rho)$, $\boldsymbol{\psi}^{(+)}(\rho)$ are matrix solutions of the homogeneous coupled equations [Eq. (9) without the source term] satisfying the following asymptotic conditions at $\rho\to\infty$:

$$\boldsymbol{\psi}^{(\mathrm{r})}(\rho) \sim \boldsymbol{\psi}^{(-)}(\rho) - \boldsymbol{\psi}^{(+)}(\rho)\mathbf{S}, \tag{16a}$$

$$\psi_{\nu\nu'}^{(\pm)}(\rho) \sim \sqrt{\frac{\mu_\rho}{K_\nu}}\exp(\pm iK_\nu\rho)\delta_{\nu\nu'}. \tag{16b}$$

Here $\mathbf{S}$ is the scattering matrix. According to the standard definition of the scattering matrix, the solutions $\boldsymbol{\psi}^{(\pm)}(\rho)$ are normalized to the unit flux in each channel. According to Eqs. (16a) and (16b), the required asymptotic factor in Eq. (13) is

$$\lim_{\rho\to\infty}|\psi_\nu(\rho)|^2 = \frac{|B_\nu|^2}{4\mu_\rho K_\nu}, \tag{17}$$

where coefficients $B_\nu$ are given by the following matrix equation:

$$\mathbf{B} = \int_0^\infty \boldsymbol{\psi}^{(\mathrm{r})T}(\rho')\boldsymbol{\lambda}(\rho')d\rho'. \tag{18}$$

To find the matrix $\boldsymbol{\psi}^{(\mathrm{r})}(\rho)$, we first integrate outward the homogeneous system of coupled equations corresponding to Eq. (9) with the regular boundary conditions at the origin.

TABLE I. The harmonic frequencies (in $cm^{-1}$) of the $CF_3Cl$ calculated using our two-dimensional Hamiltonian, the frequency of the umbrella mode of the $CF_3$ radical, and their comparison with experimental data.

| | Our Hamiltonian | Experiment |
|---|---|---|
| $\omega_2$ | 775.12 | 862.18 [29] |
| $\omega_3$ | 463.33 | 483.07 [29] |
| $CF_3$ fragment ($\omega_2$) | 747.38 | $701 \pm 3$ [30] |

We form the square matrix of the solutions $\boldsymbol{\psi}^{(\mathbf{a})}(\rho_0)$ at some intermediate distance $\rho=\rho_0$. Similarly, we obtain the solutions $\boldsymbol{\psi}^{(\pm)}(\rho)$ by the inward integration of the homogeneous coupled system of equations corresponding to Eq. (9) from the asymptotic region to $\rho=\rho_0$, where we again form the matrix of solutions satisfying the asymptotic conditions (16a) and (16b). We match this matrix with the matrix $\boldsymbol{\psi}^{(\mathbf{a})}(\rho_0)$ to find the solution of the homogeneous system satisfying both boundary conditions using the equation

$$\boldsymbol{\psi}^{(\mathbf{a})}(\rho_0)\mathbf{C} = \boldsymbol{\psi}^{(-)}(\rho_0) - \boldsymbol{\psi}^{(+)}(\rho_0)\mathbf{S} \tag{19}$$

and similar for the derivatives of the solutions. Here $\mathbf{C}$ is a matrix of coefficients which should be determined together with the $\mathbf{S}$ matrix from the matching conditions. Since the exponentially growing solutions in the closed channels are unphysical, matrices $\mathbf{C}$, $\boldsymbol{\psi}^{(-)}(\rho_0)$, and $\mathbf{S}$ are rectangular with $N$ rows and $N_0$ columns, where $N$ is the total number of the vibrational channels and $N_0$ is the number of the open channels. After $\mathbf{S}$ and $\mathbf{C}$ are found, the column $\mathbf{B}$ is calculated as

$$\mathbf{B} = \int_0^{\rho_0} \mathbf{C}^T \boldsymbol{\psi}^{(\mathbf{a})T}(\rho)\boldsymbol{\lambda}(\rho)d\rho + \int_{\rho_0}^{\infty} [\boldsymbol{\psi}^{(-)T}(\rho) - \mathbf{S}\boldsymbol{\psi}^{(+)T}(\rho)]\boldsymbol{\lambda}(\rho)d\rho. \tag{20}$$

## III. CALCULATIONS

In our multimode calculations we used the two-dimensional surfaces of $CF_3Cl$ and the corresponding anion calculated by the second-order Møller-Plesset perturbation theory [24]. All calculations were performed with GAUSSIAN 03 suite of codes [25] employing the Dunning's augmented correlation-consistent polarized valence-triple-zeta (cc-pVTZ) basis set [26–28]. More details are given in Ref. [5].

Since we use the two-mode approximation for the vibrational wave functions in all our calculations, it is useful to check how well our two-dimensional Hamiltonian with the potential surface of the neutral molecule reproduces the corresponding normal-mode frequencies. Comparison of our results with experimental data due to Scanlon *et al.* [29] is given in Table I. As can be seen, our two-dimensional Hamiltonian gives slightly underestimated values for the normal-modes frequencies but they are still in good agreement with experiment and justify the use of our two-dimensional treatment of the neutral $CF_3Cl$.

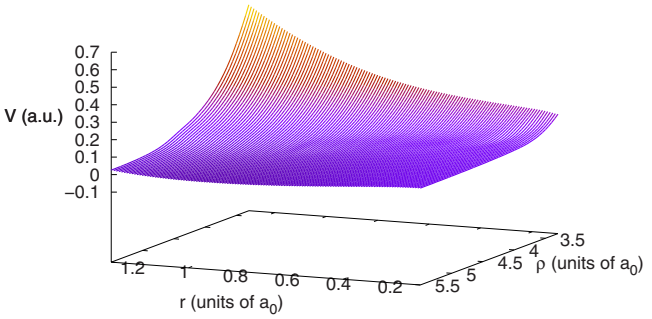


FIG. 1. (Color online) The two-dimensional anionic potential surface used in the multimode calculations. The zero potential corresponds to the minimum of the neutral target potential surface.

For the anion at $R<1.9$ Å the present calculation exhibits a kinklike behavior similar to that observed in the previously published one-dimensional calculation [14], where it was explained by variational collapse: an attempt to introduce a more diffuse basis set leads to larger contribution of the continuum states and the "collapse" of the anion energy to the neutral energy (with the zero-energy electron in the continuum). In order to remove this deficiency, we employed a semiempirical method used in several previously published calculations [13,14]: we extrapolated the calculated anionic potential surface toward smaller $R$ so that it represents the correct vertical attachment energy, 1.83 eV, in the case of $CF_3Cl$ [21]. The adjusted surface is plotted in Fig. 1.

In our multimode calculations the $CF_3$ fragment was represented by the potential curve $V(\infty,r)$ plotted in Fig. 2. The potential could be symmetrically continued toward negative values of $r$ due to possible flip-flop of the $CF_3$ radical. However, in the present work we restrict our considerations to geometries of $CF_3$ which do not exceed the planar configuration. As can be seen in Table I, the fixation of the C-F bond in our treatment gives slightly higher vibrational frequency than previous experimental study [30].

In order to find the asymptotic solution of system of equations (9) we need to evaluate potential matrix (10) also for values of $R$ and $r$ exceeding the region in which the quantum

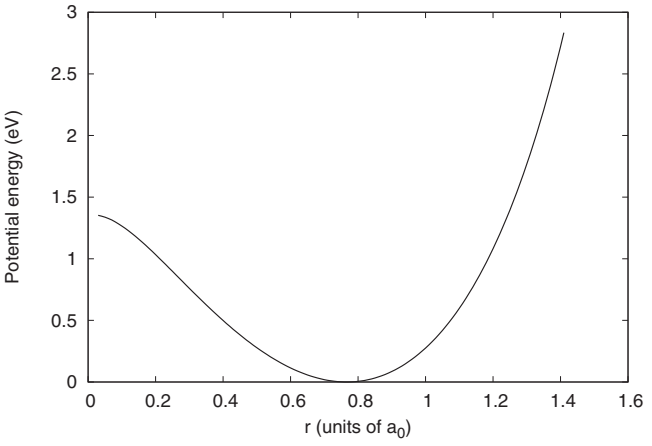


FIG. 2. The potential energy of the $CF_3$ radical as a function of the distance between the carbon atom and the plane of the fluorine atoms.

TABLE II. Parameters of the Morse potentials (in a.u.) used in our one-dimensional calculations taken from Ref. [14].

| | $\beta$ (units of $a_0^{-1}$) | $B$ (a.u.) | $C$ (a.u.) | $D$ (a.u.) |
|---|---|---|---|---|
| Neutral molecule | 0.8507 | 0.1382 | 0.2764 | 0.1382 |
| Negative ion | 0.820 | 0.0928 | 0.009 | −0.011 |

chemical calculation of the potential surfaces is available. Since the imaginary part of the potential matrix $U_{\nu\nu'}(\rho)$ vanishes outside this region, it is necessary to continue the anionic surface only. To this end we introduced the following parametrization of the surface:

$$U(R,r) = b(r)\exp[-2\beta(r)(R-R_0)] - c(r)\exp[-\beta(r)(R-R_0)] + V(\infty,r) - V(\infty,r_m) + D_e - E_a, \quad (21)$$

where $r_m=0.77$ $a_0$ is the position of the minimum of the $CF_3$ radical potential energy $V(\infty,r)$, $D_e=4.014$ eV is the C-Cl bond dissociation energy [5], and $E_a=3.613$ eV is the electron affinity of the Cl atom [31]. This parametrization reproduces correct asymptotic behavior in $R$ of the anionic potential. For every fixed $r$ it represents the Morse potential, the parameters $\beta(r)$, $b(r)$, and $c(r)$ are determined by the condition of the smooth connection between the region where the potential is given by quantum chemical calculation and the region where we use the parametrization.

In order to justify the use of the local theory of the DEA and to see the effect of the vibrational modes of the $CF_3$ radical we performed two local one-dimensional calculations [18–20] with fixed $CF_3$ radical. In the first calculation we used the Morse potentials

$$U_M(R) = B\exp[-2\beta(R-R_0)] - C\exp[-\beta(R-R_0)] + D \quad (22)$$

for the neutral and anionic curves as functions of the C-Cl distance. In both cases $R_0=3.307$ $a_0$ was taken and it corresponds to the position of the neutral potential surface minimum. These potentials were used previously by Wilde *et al.* [14] in the nonlocal semiempirical $R$-matrix calculation and corresponding parameters are given in Table II.

The parameters of the neutral potential were chosen to reproduce the experimental value of the vibrational frequency [29] and the anionic potential curve was obtained by fitting to the *ab initio* calculations [14]. Another one-dimensional calculation was performed using the potential curves extracted from our two-dimensional surfaces. We took the potential curves along $R$ in the neutral and anionic surfaces with fixed $r=0.877$ $a_0$ corresponding to the value at the minimum of the neutral potential surface. These curves are compared with the Morse potentials in Fig. 3.

This graph shows that the different behavior in the vicinity of the crossing points of the neutral potential curve with the corresponding anionic potential leads to slightly different position of these crossing points. While in the case of the Morse potentials $R_C=3.87$ $a_0$, the potential curves extracted from the two-dimensional surface give the value $R_C=3.80$ $a_0$. We do not expect that the different behavior at larger C-Cl internuclear separation will have considerable influence on the DEA cross sections.

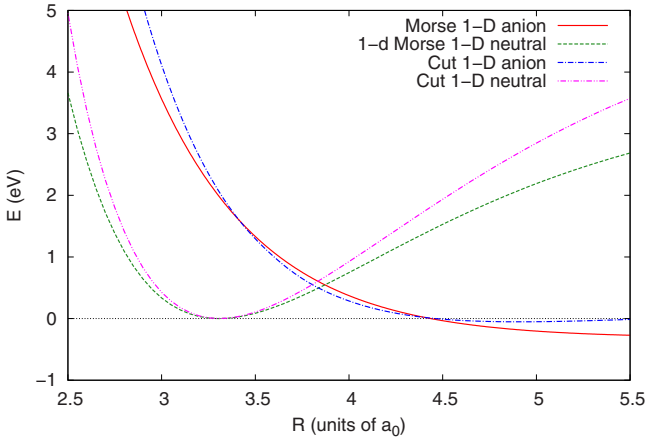


FIG. 3. (Color online) Potentials used in the one-dimensional calculations. The Morse potentials taken from [14] are compared with curves extracted from the two-dimensional surfaces.

All our calculations discussed in the present work employed the width function obtained from the semiempirical $R$-matrix theory as described in [14]. In this study, the surface amplitude of the semiempirical one-pole $R$ matrix was fitted to the experimental vibrational excitation cross section of Mann and Linder [7]. As a result, the energy-dependent fixed-nuclei resonance width can be calculated using the general relation between the surface amplitude and the resonance width [32]. In the one-dimensional local calculations the local (adiabatic) width is represented as $\Gamma(E_r(R),R)$, where $E_r(R)=U(R)-V(R)$ is the resonance energy for a given C-Cl internuclear separation $R$. Its extension to the two-dimensional case requires an additional information on the dependence of the width on the second coordinate $r$. As a first step, we present here the two-dimensional width $\Gamma(E_r(R,r),R,r)$ as a function of $E_r(R,r)$ only. This function is plotted in Fig. 4.

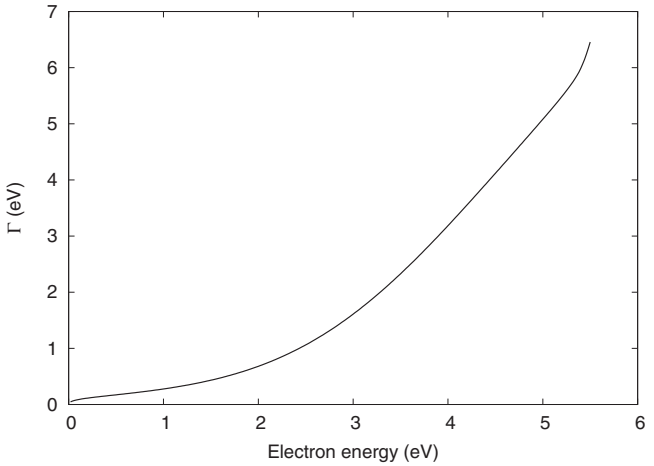


FIG. 4. The width function Γ used in our calculations taken from the nonlocal semiempirical $R$-matrix calculation [14].

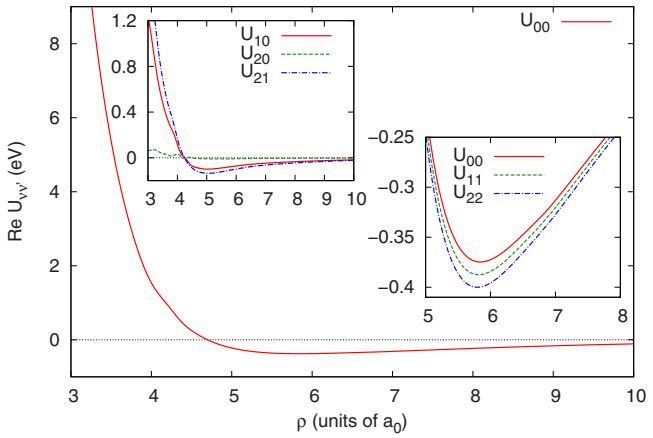


FIG. 5. (Color online) The lowest diagonal and off-diagonal elements of the real part of the potential matrix $U_{\nu\nu'}(\rho)$.

Near the threshold $\Gamma(E_r)$ exhibits the $s$-wave behavior slightly modified by a small permanent dipole moment (0.5 D). For larger $E_r$ the behavior is more consistent with the $E^{3/2}$ dependence typical for $\sigma^*$ resonances [21].

Using the potential surfaces and widths discussed above we calculated potential matrix (10). Few lowest elements (as functions of $\rho$) are plotted in Figs. 5 and 6.

The lowest diagonal elements are very similar to each other and the most pronounced differences between them appear in the region around their minima. However, due to the oscillatory character of the vibrational wave functions $\phi_s(r)$, $\phi_{s'}(r)$, the off-diagonal elements become smaller with increasing difference between the indices $s$ and $s'$.

The system of differential equations (9) was integrated as discussed in Sec. II B using Milne's predictor-corrector method [33]. We employed this technique since it does not require the calculation of the first derivatives of the solution. To use this method it is necessary to have the solution corresponding to first four steps in the integration region. To this end we calculated the semiclassical wave functions [34] corresponding to the real part of potential matrix (10) deep enough in the classically forbidden region. This solution evaluated at four lowest steps of the outward integration was

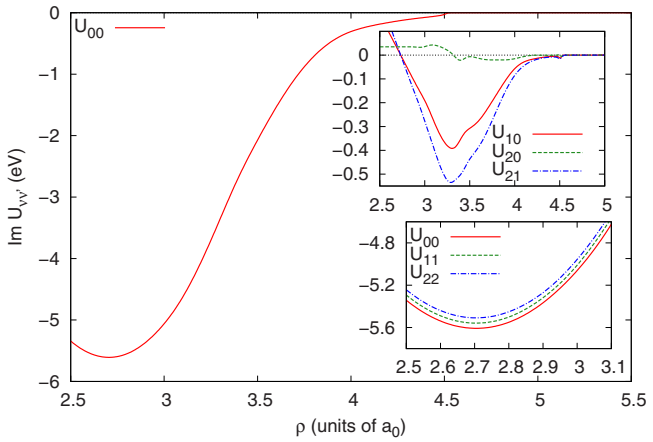


FIG. 6. (Color online) The lowest diagonal and off-diagonal elements of the imaginary part of the potential matrix $U_{\nu\nu'}(\rho)$.

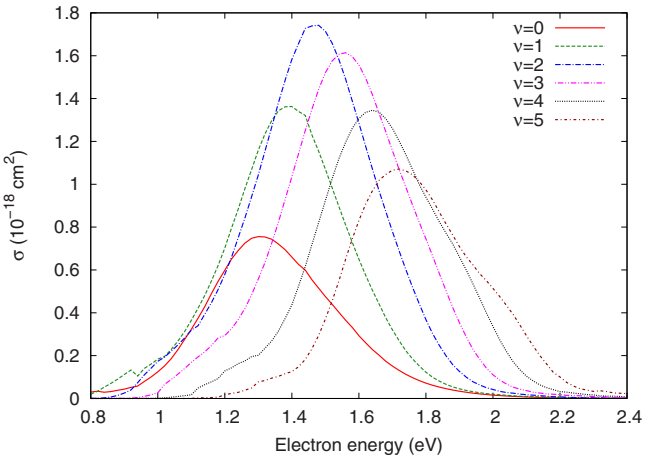


FIG. 7. (Color online) DEA cross sections obtained from the two-dimensional calculation for different final vibrational states of the fragment $CF_3$. The curves with peaks at higher energies correspond to higher vibrational states of the $CF_3$ fragment.

used to integrate the full system of equations (9). The small values of the semiclassical wave functions in the classically forbidden region enabled us to neglect the imaginary part of potential matrix (10). This method showed to be stable with respect to change of the starting point of the outward integration as far as it was far enough from the corresponding classical turning point. The inward integration was started in the region where potential matrix (10) can be neglected and where solutions satisfying conditions (16a) and (16b) can be used to start the predictor-corrector integration.

Since we start the outward integration in the classically forbidden region, the solutions of the homogeneous system of equations corresponding to Eq. (9) raise rather rapidly with increasing $\rho$ in this region, especially in the case of energetically closed channels. In this case the exponentially increasing component of the solution becomes dominant and the linear dependence with the exponentially decreasing component raises the issues with the matching procedure described above. In order to keep the calculations numerically tractable, we did not include more than one closed channel into our calculations for every particular energy of the interest. However, the large masses of the nuclei suggest that the inclusion of the closed channels will not influence the results significantly.

## IV. RESULTS

### A. Local complex potential calculations

We performed the multimode calculation of the cross sections for the DEA to $CF_3Cl$ in the ground vibrational state for initial electron energies from 0.8 to 3 eV. Using the basis set of 13 lowest vibrational wave functions of $CF_3$ to solve Eq. (9) we obtained converged results for final states of the fragment with vibrational quantum numbers $\nu \leq 6$ as well as converged total cross section. Due to the restriction to one closed channel only discussed above, the cross sections at energies with less than 12 open channels ($E < 1.48$ eV) were calculated using the smaller basis sets. The distribution of

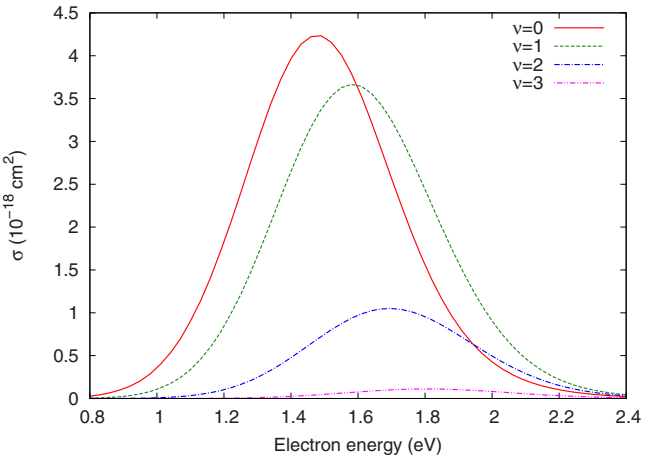


FIG. 8. (Color online) DEA cross sections obtained from the two-dimensional model for different final vibrational states calculated using the diagonal elements of potential matrix (10) only.

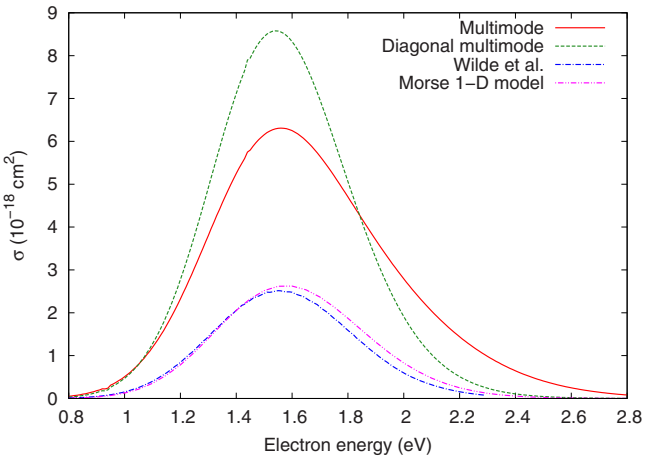


FIG. 9. (Color online) Comparison of the total DEA cross section corresponding to the multimode calculation (multimode) with calculation neglecting the off-diagonal elements of potential matrix (10) (diagonal multimode), with one-dimensional model using the Morse potentials [14] (Morse 1D model) and with previously published calculations [14].

final vibrational states of the $CF_3$ fragment is plotted in Fig. 7.

This graph shows that the cross section with the highest peak corresponds to the final vibrational state of the fragment with $\nu=2$. For every energy in the range of our interest the cross section corresponding to $\nu=0$ is below the cross section for $\nu=1$. This suggests that the DEA to $CF_3Cl$ is an efficient way of vibrational excitation of $CF_3$. These results can be understood by analyzing two mechanisms taking place in the DEA: the vertical Franck-Condon transition and final-state interaction. The vertical transition leaves the $CF_3$ radical in a particular vibrational state. Then the $CF_3$ umbrella motion is influenced by the $Cl^-$ ion in the temporal anionic complex, and as a consequence of this final-state interaction, the vibrational state of the fragment can be changed. In order to analyze the relative importance of these two mechanisms in production of the excited fragments, we performed another calculation where we neglected all the off-diagonal elements in potential matrix (10). Therefore, the coupling between different vibrational states of the radical due to the interaction with the $Cl^-$ ion in Eq. (9) was not taken into account. Results of this calculation are plotted in Fig. 8.

As can be seen in this graph, the dominant cross sections correspond to the vibrational ground state ($\nu=0$) and first excited state of the fragment ($\nu=1$). All the peaks corresponding to higher excited states are successively decreasing with raising $\nu$. Comparison of Fig. 7 with Fig. 8 shows that dominance of the cross section corresponding to $\nu=2$ around its peak is mainly due to interaction of the umbrella motion with the $Cl^-$ ion in the anionic complex. As can be seen in Fig. 9, the reduction in the excited fragments due to the neglect of the coupling leads to a narrower peak in the total cross section when compared with calculation including the off-diagonal elements of potential matrix (10). This figure shows that our two-dimensional calculations give rather high total DEA cross sections when compared with previous studies [14].

In order to understand these results, we performed two one-dimensional LCP calculations using the Morse potentials described above and using the potential curves taken from the two-dimensional potential surfaces as discussed in Sec. III. Corresponding cross sections are plotted in Fig. 10.

It shows that the model using the potentials extracted from the two-dimensional surfaces gives cross section larger approximately by a factor of 2 than the cross section calculated using the Morse potentials. The peaks, however, appear at very close energy of about 1.65 or 1.7 eV. As can be seen in Fig. 10, our one-dimensional calculation using the Morse potentials is in very good agreement with previously published results of the nonlocal semiempirical $R$-matrix calculations [14]. This agreement justifies the use of the local theory. The same figure shows the comparison with previous nonlocal calculation due to Beyer *et al.* [15]. The fixed nuclei quantities used to construct the nonlocal model in Ref. [15]

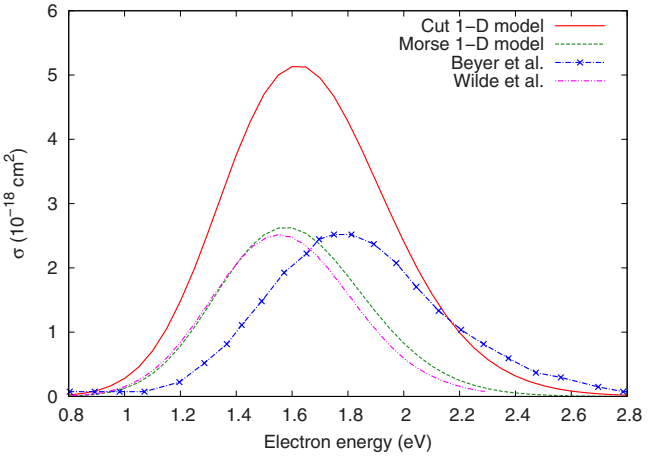


FIG. 10. (Color online) Comparison of the DEA cross section corresponding to the one-dimensional model using the potential extracted from the two-dimensional surface (cut 1D model) with model using the Morse potentials [16] (Morse 1D model) and with previously published one-dimensional nonlocal calculations by Wilde *et al.* [14] and Beyer *et al.* [15].

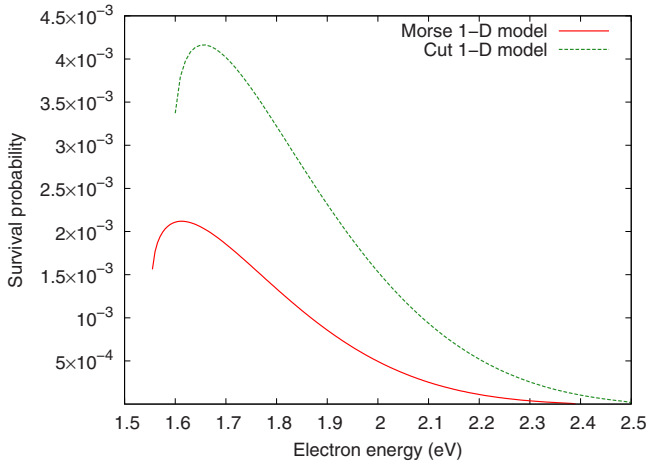


FIG. 11. (Color online) Survival probability calculated for the one-dimensional model using the Morse potential (Morse 1D model) is compared with the one-dimensional model using the potential extracted from the two-dimensional surface (cut 1D model).

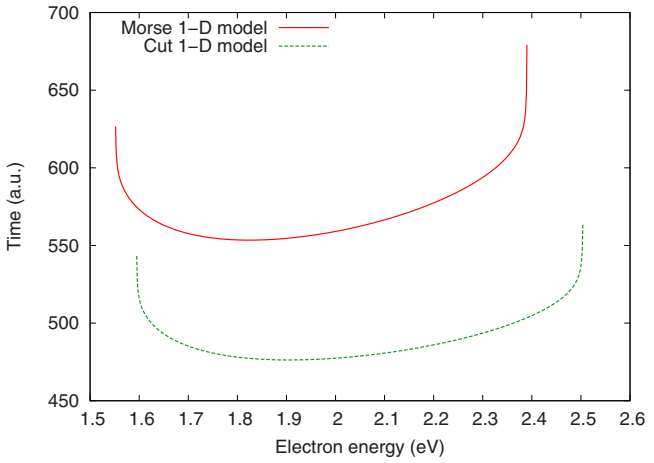


FIG. 12. (Color online) Stabilization time calculated for the one-dimensional model using the Morse potential (Morse 1D model) is compared with the one-dimensional model using the potential extracted from the two-dimensional surface (cut 1D model).

were obtained from the *ab initio* $R$-matrix calculations [35]. It can be seen that these results are in good correspondence to our calculations using the Morse potentials. However, the peak in our results appears at energy which is 0.15 eV below the peak position in Ref. [15] and its value is 0.004 Å$^2$ lower. This difference also can be attributed to different treatments of the resonant anionic state.

### B. Classical calculations

To emphasize how the differences in potentials used in our one-dimensional calculations change the cross sections, we calculated the survival probability $\mathcal{P}$ of the negative ionic complex [36] for both models using the formula

$$\mathcal{P}(E) = \exp\left[ - \sqrt{\frac{\mu_\rho}{2}} \int_{R_F(E)}^{R_C} \frac{\Gamma(R) dR}{\sqrt{E - U(R)}} \right], \tag{23}$$

where $R_C$ is the crossing point of the anionic potential curve with the neutral potential. $R_F(E)$ is the Franck-Condon point given by the condition [37]

$$U(R_F(E)) - V(R_F(E)) = E - E_{\text{vib}}, \tag{24}$$

where $E_{\text{vib}}$ is the corresponding vibrational energy of the neutral molecule. Calculated survival probabilities are plotted in Fig. 11.

This graph shows that the curve corresponding to the model using Morse potentials is smaller by a factor of 2 than the curve using the potentials extracted from the two-dimensional surfaces. This result corresponds to the DEA cross sections plotted in Fig. 10. Since we use the same resonance width $\Gamma(R)$ in both models, the difference arises from the different time needed to pass from $R_F(E)$ to $R_C$ on the anionic curve for given electron energy. This time, given by the formula

$$T(E) = \sqrt{\frac{\mu_\rho}{2}} \int_{R_F(E)}^{R_C} \frac{dR}{\sqrt{E - U(R)}}, \tag{25}$$

is plotted in Fig. 12 for both one-dimensional models.

It shows that this time for Morse model is higher than for the model using the potentials extracted from the two-dimensional surface for every energy. These results suggest that the small differences in the potentials used in our models lead to rather large changes in the corresponding DEA cross sections. The more extensive discussion of the character of the stabilization time $T(E)$ and its relation with the maximum of the survival probability is presented in the Appendix.

It is an interesting feature of the results obtained from our two-dimensional LCP calculation that it exhibits a substantial increase in the total cross section when compared with the one-dimensional case. This is partly because of more favorable potential surfaces intersection in the multimode calculation. As has been shown, the one-dimensional potential curve extracted from the two-dimensional surface produces a higher survival probability. In the case of the two-dimensional potential surface, the negative ion motion can be even more favorable (in terms of the survival probability). To understand this better, we have performed classical simulations of the DEA process along the lines developed in Ref. [38] (see also Ref. [39]).

The classical DEA cross section can be written as

$$\sigma = \frac{2\pi^2}{k_i^2} \int d\mathbf{P} d\mathbf{Q} \Gamma(\mathbf{Q}) W[\mathbf{q}(\mathbf{Q},\mathbf{P}), \mathbf{p}(\mathbf{Q},\mathbf{P})] \times \delta[H(\mathbf{Q},\mathbf{P}) - E] \mathcal{P}(\mathbf{Q},\mathbf{P}), \tag{26}$$

where $\mathbf{Q},\mathbf{P}$ are the sets of initial reaction coordinates and conjugated momenta, $\Gamma(\mathbf{Q})$ is the adiabatic width function, $W(\mathbf{q},\mathbf{p})$ is the Wigner distribution function expressed in terms of the set of normal coordinates $\mathbf{q}$ and conjugated momenta $\mathbf{p}$, $H(\mathbf{Q},\mathbf{P})$ is the classical Hamiltonian of the system, and $\mathcal{P}(\mathbf{Q},\mathbf{P})$ is the survival factor given by $\mathcal{P}=\exp[-\int \Gamma(t) dt]$ along the classical trajectory corresponding to the initial coordinates $\mathbf{Q}$ and momentum $\mathbf{P}$.

For interpretation of our two-dimensional LCP results we analyzed several classical trajectories which give the most

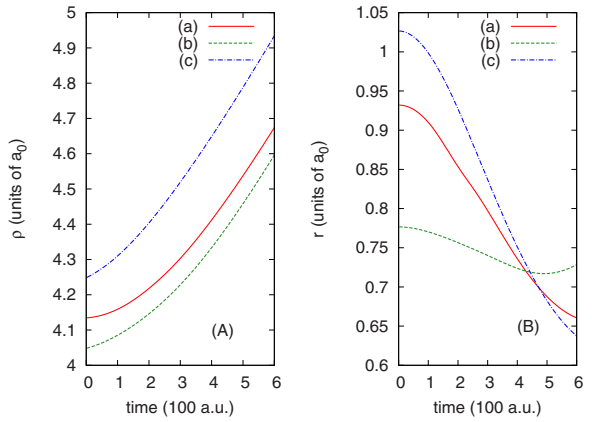


FIG. 13. (Color online) (a) The reaction coordinate $\rho$ and (b) the reaction coordinate $r$ as functions of time obtained from the classical two-dimensional calculation corresponding to the initial conditions listed in Table III.

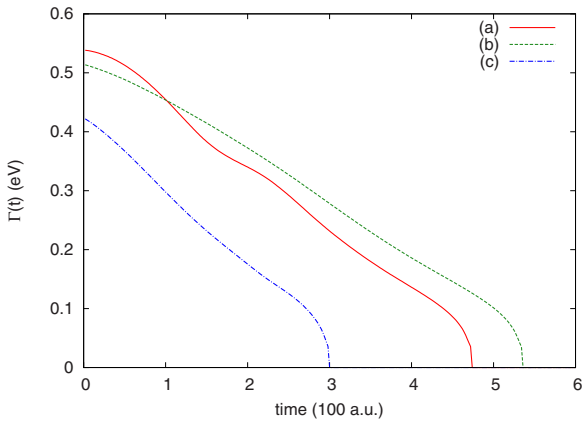


FIG. 14. (Color online) Resonance width as a function of time for the trajectories presented in Fig. 13 calculated using the initial conditions listed in Table III.

significant contribution to integral (26). They correspond to the maximum of the function

$$F(\mathbf{Q},\mathbf{P}) = W[\mathbf{q}(\mathbf{Q},\mathbf{P}),\mathbf{p}(\mathbf{Q},\mathbf{P})]\mathcal{P}(\mathbf{Q},\mathbf{P}) \tag{27}$$

with the constraint imposed by the conservation of energy

$$H(\mathbf{Q},\mathbf{P}) = E. \tag{28}$$

In our case of 2 degrees of freedom, we have three independent parameters corresponding to the initial conditions. We have chosen $\rho$, $r$, $p_r$, with $p_\rho$ defined by Eq. (28).

In Figs. 13 and 14 we present the time dependence of $\rho$, $r$, and $\Gamma$ for three classical trajectories with relatively high values of the function $F(\mathbf{Q},\mathbf{P})$. The incident electron energy is 1.7 eV and the corresponding initial positions and momenta are presented in Table III. Note that the case (a) corresponds to the maximum value of the function $F$, whereas case (c) to the maximum value of the survival probability. However, in case (c) the value of the Wigner distribution function is very low.

From the analysis of Figs. 13 and 14 we see that the optimal classical trajectory does not correspond to a constant value of $r$, therefore by going from one-dimensional to two-dimensional case we have more possibilities to increase the survival factor by expanding the class of possible trajectories. Typically optimal trajectories lead to substantially higher survival probabilities than we obtain in the one-dimensional case. Note, however, that, although this conclusion is qualitatively general, the quantitative results depend on the width function $\Gamma(\mathbf{Q})$, and in the present case the width is rather arbitrarily (although reasonably) extended from one-dimensional case to two-dimensional case.

## V. CONCLUSIONS

We performed a two-dimensional LCP calculation of the DEA to $CF_3Cl$ in the ground vibrational state at energies from 0.8 to 3 eV. The corresponding total cross section exhibits a substantial increase when compared with our one-dimensional models and previously published studies. Our classical two-dimensional calculation showed that this is due to the more optimal, with respect to the survival probability, paths performed by the final products in the two-dimensional case compared to those in the one-dimensional case. The classical trajectories with largest contribution to the DEA cross section do not correspond either to a fixed value of the coordinate $r$ or optimal (in the sense of the minimal energy) path in the $(\rho,r)$ plane. This suggests that the additional degree of freedom enables the increase in the DEA cross section. With the increasing number of vibrational degrees of freedom quantum-mechanical calculations become computationally very demanding, therefore a further development of classical and semiclassical methods [38–41] is necessary.

The results obtained for the distribution of the final vibrational states of the $CF_3$ radical show that the cross section with the highest peak corresponds to the vibrational state of the $CF_3$ fragment with $\nu$=2. We showed that this excitation is mainly due to the final-state interaction, leading to the energy exchange between the umbrella motion and the C-Cl

TABLE III. Parameters of classical trajectories presented in Figs. 13 and 14, together with corresponding value of the function $F$ and the survival factor $S$. Initial coordinates and momenta are given in a.u., and function $F$ in arbitrary units.

| | $\rho$ | $r$ | $P_\rho$ | $P_r$ | $F$ | $S$ |
|---|---|---|---|---|---|---|
| (a) | 4.134 | 0.932 | 2.611 | 0.103 | 1.000 | 0.0050 |
| (b) | 4.048 | 0.777 | 10.275 | −0.100 | 0.0605 | 0.0026 |
| (c) | 4.248 | 1.027 | 18.777 | −0.100 | 0.00095 | 0.0727 |

motion in the temporal anionic complex. Therefore, our results support the findings indicating the importance of the $CF_3$ vibrational energy redistribution during the DEA at higher energies [9–11].

Our new cross sections for attachment to the ground state of $CF_3Cl$ are about a factor of 3 higher than those calculated within the framework of one-dimensional model. This also leads to worse agreement with experiment at room temperature [16,21,42,43] when only ground vibrational state of $CF_3Cl$ is mostly populated. However, our width has been extrapolated from an empirical width obtained from one-dimensional calculations. For a proper comparison with experiment the two-dimensional adiabatic width should be calculated *ab initio*, or readjusted with the account of the second vibrational coordinate. As a next step, we plan calculations of vibrational excitation cross sections which would allow us to obtain a semiempirical two-dimensional width by its adjustment to experimental data [7] on vibrational excitation.

The next step will be the extension of our calculations of DEA to vibrationally excited states. This will allow us to study the temperature dependence of DEA cross sections and hopefully will explain the low-energy peak at 800 K [16] which cannot be explained by existing one-dimensional calculations [14,15].

## ACKNOWLEDGMENTS

This work was partially supported by the National Science Foundation under Grant No. PHY-0652866, by Grant No. GAUK 116-10/257718 of the Charles University Prague and by the Center of Theoretical Astrophysics Grant No. LC06014 of the Ministry of Education, Youth, and Sports of the Czech Republic.

## APPENDIX: DISCUSSION OF THE MAXIMUM OF THE SURVIVAL PROBABILITY

Here we will discuss the origin of the unexpected maximum of the survival probabilities shown in Fig. 11. The decreasing part of each curve corresponds to the raising parts of $T(E)$ plotted in Fig. 12. Since the temporal anionic system (treated classically) needs longer time to reach the stabilization point $R_C$, the survival probability decreases with raising energy. The increasing part at the smaller energies corresponds to the rapidly decreasing parts of the curves $T(E)$ plotted in Fig. 12. As a consequence of Eqs. (24) and (25), the larger energy leads to shift of the Franck-Condon point toward smaller values and prolongs the classical path of the anionic system to the stabilization point $R_C$ (see Fig. 15). However, this time increase competes with increase in the classical velocity. Let us investigate the behavior of $T(E)$ in the limit of energies sufficiently close to $E_2=U(R_2)-V(R_2)+E_{\mathrm{vib}}$, where $R_2$ is the right boundary of the Franck-Condon region of the ground vibrational state (see Fig. 15).

$E_2$ provides the left boundary of energies for which it is possible to define the survival probability. Consider $E$ close to $E_2$, so that anionic turning point $R_t$, determined by the condition $U(R_t)=E$, can be approximated by a linear function of $E$,

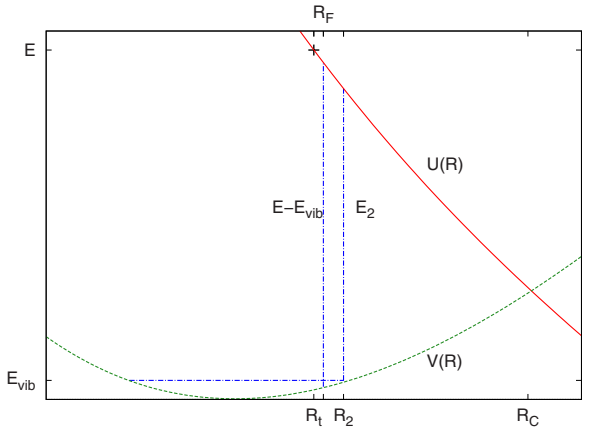


FIG. 15. (Color online) The relative positions of the turning point $R_t$, Franck-Condon point $R_F$ and the crossing point $R_C$, and corresponding energies used in the calculations of the survival probabilities $\mathcal{P}(E)$ and times $T(E)$.

$$R_t = R_2 + d(E_2 - E), \tag{A1}$$

where $d>0$ is the constant dependent on the potentials in the vicinity of $R_2$. As the energy $E$ decreases toward $E_2$, the corresponding Franck-Condon point $R_F$ shifts toward $R_2$ as well as $R_t$ (see Fig. 15) and can be approximated as

$$R_F = R_2 + b(E_2 - E), \tag{A2}$$

where $0<b<d$, since $R_t<R_F$. These approximations are equivalent to the assumption that the kinetic energy for the motion in the anion potential between $R_t(E)$ and $R_2$ can be approximated by a linear function. Then we can write

$$E - U(R) \approx c(R - R_t), \tag{A3}$$

where $c>0$ is another constant dependent on the behavior of the anionic potential between $R_t$ and $R_2$. Using these assumptions we can express integral (25) for energies sufficiently close to $E_2$ as follows:

$$T(E) = \sqrt{\frac{\mu_\rho}{2c}} \int_{R_F(E)}^{R_2+\varepsilon} \frac{dR}{\sqrt{R - R_t}} + \sqrt{\frac{\mu_\rho}{2}} \int_{R_2+\varepsilon}^{R_C} \frac{dR}{\sqrt{E - U(R)}}, \tag{A4}$$

where $\varepsilon>0$ is a constant small enough to make approximation (A3) valid at the interval $\langle R_t, R_2+\varepsilon\rangle$. Then we can calculate the first integral in Eq. (A4) and obtain

$$T(E) = 2\sqrt{\frac{\mu_\rho}{2c}}\{\sqrt{d(E - E_2) + \varepsilon} - \sqrt{(d-b)(E - E_2)}\} + \sqrt{\frac{\mu_\rho}{2}} \int_{R_2+\varepsilon}^{R_C} \frac{dR}{\sqrt{E - U(R)}}. \tag{A5}$$

This equation shows that $T$ as a function of $E$ exhibits a square-root singularity of the type const$-p\sqrt{E-E_2}$ where $p$ is a positive constant. Therefore, when $E$ starts to increase from $E_2$, $T(E)$ is always decreasing and reaches a minimum at higher $E$. Therefore the survival probability increases first and then reaches a maximum as can be seen in Fig. 11. Note that this result is not valid if $R_C=R_2$.


[1] A. Kazansky, J. Phys. B **28**, 3987 (1995).
[2] D. J. Haxton, Z. Zhang, H.-D. Meyer, T. N. Rescigno, and C. W. McCurdy, Phys. Rev. A **69**, 062714 (2004).
[3] S. T. Chourou and A. E. Orel, Phys. Rev. A **77**, 042709 (2008).
[4] M. Shapiro and R. Bersohn, J. Chem. Phys. **73**, 3810 (1980).
[5] S. Roszak, W. S. Koski, J. J. Kaufman, and K. Balasubramanian, J. Chem. Phys. **106**, 7709 (1997).
[6] A. Gedanken and M. D. Rowe, Chem. Phys. Lett. **34**, 39 (1975).
[7] A. Mann and F. Linder, J. Phys. B **25**, 1621 (1992).
[8] C. W. Walter, B. G. Lindsay, K. A. Smith, and F. B. Dunning, Chem. Phys. Lett. **154**, 409 (1989).
[9] A. Kalamarides, C. W. Walter, B. G. Lindsay, K. A. Smith, and F. B. Dunning, J. Chem. Phys. **91**, 4411 (1989).
[10] A. Kalamarides, R. W. Marawar, X. Ling, C. W. Walter, B. G. Lindsay, K. A. Smith, and F. B. Dunning, J. Chem. Phys. **92**, 1672 (1990).
[11] R. Parthasarathy, C. D. Finch, J. Wolfgang, P. Nordlander, and F. B. Dunning, J. Chem. Phys. **109**, 8829 (1998).
[12] D. M. Pearl, P. D. Burrow, I. I. Fabrikant, and G. A. Gallup, J. Chem. Phys. **102**, 2737 (1995).
[13] R. S. Wilde, G. A. Gallup, and I. I. Fabrikant, J. Phys. B **33**, 5479 (2000).
[14] R. S. Wilde, G. A. Gallup, and I. I. Fabrikant, J. Phys. B **32**, 663 (1999).
[15] T. Beyer, B. M. Nestmann, and S. D. Peyerimhoff, J. Phys. B **34**, 3703 (2001).
[16] I. Hahndorf, E. Illenberger, L. Lehr, and J. Manz, Chem. Phys. Lett. **231**, 460 (1994).
[17] S. Marienfeld, T. Sunagawa, I. I. Fabrikant, M. Braun, M.-W. Ruf, and H. Hotop, J. Chem. Phys. **124**, 154316 (2006).
[18] J. N. Bardsley, A. Herzenberg, and F. Mandl, Proc. Phys. Soc. **89**, 305 (1966).
[19] J. N. Bardsley, A. Herzenberg, and F. Mandl, Proc. Phys. Soc. **89**, 321 (1966).
[20] W. Domcke, Phys. Rep. **208**, 97 (1991).
[21] K. Aflatooni and P. D. Burrow, Int. J. Mass Spectrom. **205**, 149 (2001).
[22] W. H. Shaffer, J. Chem. Phys. **10**, 1 (1942).
[23] J. N. Bardsley, in *Electron-Molecule and Photon-Molecule Collisions*, edited by T. Rescigno, V. McKoy, and B. Schneider (Plenum, New York, 1979).
[24] C. Møller and M. S. Plesset, Phys. Rev. **46**, 618 (1934).
[25] M. J. Frisch, G. W. Trucks, H. B. Schlegel, G. E. Scuseria, M. A. Robb, J. R. Cheeseman, J. A. Montgomery, Jr., T. Vreven, K. N. Kudin, J. C. Burant *et al.*, *Gaussian 03, Revision C.02* (Gaussian, Inc., Wallingford, CT, 2004).
[26] J. Thom H. Dunning, J. Chem. Phys. **90**, 1007 (1989).
[27] D. E. Woon and J. Thom H. Dunning, J. Chem. Phys. **98**, 1358 (1993).
[28] A. K. Wilson, D. E. Woon, K. A. Peterson, and J. Thom H. Dunning, J. Chem. Phys. **110**, 7667 (1999).
[29] K. Scanlon, I. Suzuki, and J. Overend, J. Chem. Phys. **74**, 3735 (1981).
[30] M. Suto and N. Washida, J. Chem. Phys. **78**, 1012 (1983).
[31] R. Trainham, G. D. Fletcher, and D. J. Larson, J. Phys. B: At. Mol. Phys. **20**, L777 (1987).
[32] A. M. Lane and R. G. Thomas, Rev. Mod. Phys. **30**, 257 (1958).
[33] A. Bennett, W. E. Milne, and H. Bateman, *Numerical Integration of Differential Equations* (Dover Publications, New York, 1956).
[34] B. C. Eu, *Semiclassical Theories of Molecular Scattering* (Springer-Verlag, Berlin, 1984).
[35] B. M. Nestmann, J. Phys. B **31**, 3929 (1998).
[36] T. F. O'Malley, Phys. Rev. **150**, 14 (1966).
[37] S. A. Kalin and A. K. Kazansky, J. Phys. B **23**, 4377 (1990).
[38] S. Goursaud, M. Sizun, and F. Fiquet-Fayard, J. Chem. Phys. **65**, 5453 (1976).
[39] R. Schinke, *Photodissociation Dynamics of Small Polyatomic Molecules* (Cambridge University Press, Cambridge, 1993).
[40] L. Lehr and W. H. Miller, Chem. Phys. Lett. **250**, 515 (1996).
[41] L. Lehr, J. Manz, and W. H. Miller, Chem. Phys. **214**, 301 (1997).
[42] S. M. Spyrou and L. G. Christophorou, J. Chem. Phys. **82**, 2620 (1985).
[43] T. Underwood-Lemons, T. J. Gergel, and J. H. Moore, J. Chem. Phys. **102**, 119 (1995).